Black-Box Impedance-Based Stability Assessment of Dynamic Interactions Between Converters and Grid

Nicolás Cifuentes, *Student Member, IEEE,* Mingyu Sun, *Member, IEEE,* Robin Gupta, Bikash C. Pal, *Fellow, IEEE*

***Abstract*—This paper proposes an impedance/admittance-based methodology for stability assessment of converter-based device connections to power systems. The proposed methodology is designed to model the dynamics of detailed black-box converter models, derived from impedance frequency response measurements. From the converter's impedance frequency response measurements, a linear time-invariant (LTI) representation of its dynamics is obtained in the dq domain using a vector fitting technique. This representation is incorporated in the state-space representation of the whole power system in the dq domain, which is used to perform stability assessment considering traditional eigenvalue analysis and participation factors computation. The proposed methodology is tested in the 39 Bus New England system, including detailed models of a VSC windfarm and a modular multilevel converter (MMC) technology-based STATCOM. It has been found that the proposed impedance-based methodology is able to accurately predict the dynamic performance of black-box converter models, unstable operating conditions and converter control interactions between devices.**

***Index Terms*—Impedance-based model, Frequency response, Converter control interactions, PSCAD.**

I. Introduction

In the last decade, converter-based devices have continually increased their participation in power systems, both in the form of converter interfaced generation (CIGs) and FACT devices [1]. By simultaneously displacing conventional generation and incorporating more sophisticated control schemes however, converter-based devices can pose new risks to the stable operation of power systems. More specifically, it has been noted that these technologies can lead to system oscillations followed by unstable operation in a wide range of frequencies, from slow subsynchronous phenomena to fast control interactions of a few kHz [2], [3]. In order to investigate and analyse this unstable behaviour, impedance-based modelling of converter-based devices has gained increased attention in recent years [4]–[12].

From the design perspective, impedance-based modelling together with the generalized Nyquist criterion provide a fast method to test new control strategies and different operating conditions. It also helps to gain insight of the impact that different control loops have in the converter's dynamic response and stability. In [4], the authors use impedance modelling to assess the impact of the PLL, inner current control and outer power control loops in a VSC converter. A similar analysis is performed in [5], where the impact of the PLL and inner current control loops on the stability of a VSC is assessed. In addition, the authors demonstrate the frequency coupling effect in the dq domain introduced by the PLL scheme. Impedance-based modelling has also been used to assess the risk of control interaction and unstable operation for several converters connected to small tests grids [6]–[8].

In general, the impedance-based behaviour of a converter-based device can be obtained in two ways. From a theoretical perspective, the control and electrical equations defining the dynamics of the converter can be linearized around its operating condition. To do this, it is necessary to have full knowledge of both the control and hardware structure of the converter, together with its parameters and operating conditions [4]–[9]. From an experimental perspective, several techniques have been proposed to measure the impedance behaviour of power converters: using frequency sweep methodologies [10], [11], [13], estimate it from its transient response [14] and using MIMO parametric identification procedures [15] among others. In these cases, it is not necessary to have full knowledge of the converter structure and control schemes. Impedance measurements are thus a valuable tool to measure the dynamic behaviour of so called "Black-box" models, where the inner structure and control schemes are unknown and inaccessible.

While impedance-based models have proven useful to design and test the dynamic behaviour of converters in small test systems, it remains impractical for the stability assessment of larger power networks. This is because using the generalized Nyquist criterion or several Bode plots in larger systems to visually assess stability becomes impractical. In addition, such methods don't provide insight or the root cause of possible unstable operating conditions to power engineers and transmission system operators (TSOs), so that corrective actions can be taken. State-space models on the other hand are widely used in stability assessment studies, since they provide useful information on the cause of possible unstable operation via participation factors and eigenvalue analysis [10], [12], [16], [17]. The main problem of this approach is that a full knowledge of the system's dynamic equations is necessary, and so it remains impractical when left with black-box model of power converters [10], [12], [16], [17] for business confidential reason.

Some works have tried to fill the gap between impedance-based models and state-space approaches using system identi-

Nicolás Cifuentes and B.C. Pal are with the Department of Electrical and Electronic Engineering, Imperial College, London SW7 2AZ, U.K. (e-mail:{n.cifuentes17; b.pal}@imperial.ac.uk)

Mingyu Sun and Robin Gupta are with National Grid Electricity Transmission Plc. (e-mail:{Mingyu.Sun; Robin.Gupta}@nationalgrid.com)

fication techniques. Recent works on this topic use harmonic state-space methods to model of power electronic devices [18], [19]. Other works have focused on translating directly the impedance measurements to state-space models using model identification procedure such as the vector fitting algorithm [10], [11], [20]. In [11], the authors apply the vector fitting technique to the frequency response data of a VSC average model including a PLL, an inner current control loop and a constant DC voltage. The authors show that this approach can be use to correctly identify the eigenvalues that define the dynamic behaviour of the VSC model. In [20], the authors propose a non-parametric impedance identification procedure to assess stability and provide corrective control actions for an offshore windfarm/HVDC connection to an AC grid. While in both cases the potential of system identification techniques together with impedance modelling are showcased, an extension for stability assessment of larger grids including more complex converter models is necessary. Additionally, it has been proved that the vector fitting algorithm converges if the order of the model is chosen equal to or higher than the order of the underlying system [21], which for black-box models it is unknown. This work aims to fill the gap between impedance-based modelling and state-space stability assessment procedures for power systems. The specific contributions of this work are:

1) Provide a complete methodology to establish a state-space model for black-box converter-based models, on the basis of vector fitting techniques and frequency response data.
2) Specify how to use the vector fitting algorithm with impedance/admittance data for obtaining accurate state-space models for black-box converter in the dq domain.
3) Provide a methodology to incorporate such models in an LTI state-space model representation in the dq domain to perform stability assessment studies.
4) Validate the proposed methodology considering both average and detailed switching models of converter-based devices.
5) Test the proposed methodology in the well established 39 bus New England system, considering realistic converter-based device models.

The rest of the paper is organized as follows. Section II provides basic theoretical insight on how the impedance frequency response can be measured and modelled. Section III provides a detailed description on how to use the impedance LTI representation for stability assessment studies. Section IV provides numerical validation of the proposed methodology using EMT simulations in PSCAD. Conclusions are drawn in Section V.

II. Impedance measurement and modelling

In this section, the impedance measurement and LTI representation of black-box converter-based models is presented. Firstly, the frequency response measurement of a single converter device is presented. This is done by using a frequency sweep approach as presented in [10], [11], which is summarized in Section II-A. Secondly, a methodology to translate the frequency response data into a state-space representation for stability assessment studies is presented.

A. Frequency response measurement

To measure the frequency response of a black-box converter device using a frequency sweep approach, two conditions must be fulfilled. First, the converter-based device must be operating in steady-state behaviour. This is accomplished by connecting the converter device to an equivalent grid as shown in Fig. 1, which provides the operating conditions of the converter at the point of common coupling (PCC) as in the original AC grid. The operating conditions are defined by the grid strength at the PCC, which in this case is captured by the Thévenin equivalent impedance Z_{th} of the grid seen at the PCC, together with voltage magnitude V_0 and phase angle δ_0 provided by the infinite bus at the fundamental frequency f_0. The second condition is to provide a small-perturbation signal V_i of varying frequency f_i to measure the frequency response of the converter. In general this can be accomplished either by connecting a shunt current source or a series voltage source at the interface between the converter and the equivalent grid [11]. Since in general the grid's strength is much larger than the converter's rated power, most of the injected current will flow through the grid's impedance Z_{th} rather than through the converter. For this reason, in this work a series voltage injection V_i is considered for improved measurement accuracy.

Once the previous two conditions have been met, a frequency sweep measurement of the converter's impedance response can be performed. In the case of a single tone frequency sweep, this is achieved by varying the injected voltage signal's frequency f_i and measuring the converter's current's magnitude I_i and phase angle ψ_i at that corresponding frequency f_i. The impedance response of the converter at that specific frequency f_i can then be calculated according to (1) [11]. It is worth noting that (1) is defined in the dq domain. While the frequency sweep approach could be performed in any reference frame, the dq one is chosen in this work since it is easier to accurately track the small signals magnitudes V_i and I_i with their respective phase angles using FFT techniques, without the fundamental frequency signal interfering in the measurement since it becomes a DC value. To perform the dq transform without using a PLL in the measurement device, which would add undesired dynamics, the fundamental frequency phase angle δ_0 at the PCC can be computed beforehand using load-flow calculations. It is also important to note that, since there are 4 independent unknown variables $Z_{i,dd}$, $Z_{i,dq}$, $Z_{i,qd}$ and $Z_{i,qq}$, it is necessary to perform two measurements tests as explained in [11]. These measurements tests must be performed with linearly independent injected signals $\boldsymbol{V_{i1}}$ and $\boldsymbol{V_{i2}}$. Without loss of generality, it is possible to use a pure D and a pure Q axis injections for each test respectively, as defined in (2) (3) respectively.

$$\begin{bmatrix} Z_{i,dd} & Z_{i,dq} \\ Z_{i,qd} & Z_{i,qq} \end{bmatrix} = \begin{bmatrix} V_{i1,d} & V_{i2,d} \\ V_{i1,q} & V_{i2,q} \end{bmatrix} \begin{bmatrix} I_{i1,d} & I_{i2,d} \\ I_{i1,q} & I_{i2,q} \end{bmatrix}^{-1} \quad (1)$$

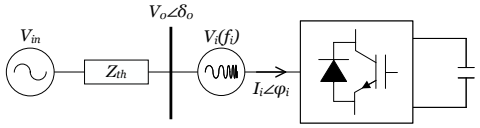


Fig. 1. Frequency sweep measurement for converter-based devices.

$$\boldsymbol{V_{i1}} = \begin{bmatrix} V_{i1} \cdot cos\left(\omega_i t\right) \\ V_{i1} \cdot cos\left(\omega_i t - \frac{2\pi}{3}\right) \\ V_{i1} \cdot cos\left(\omega_i t + \frac{2\pi}{3}\right) \end{bmatrix} \tag{2}$$

$$\boldsymbol{V_{i2}} = \begin{bmatrix} V_{i2} \cdot sin\left(\omega_i t\right) \\ V_{i2} \cdot sin\left(\omega_i t - \frac{2\pi}{3}\right) \\ V_{i2} \cdot sin\left(\omega_i t + \frac{2\pi}{3}\right) \end{bmatrix} \tag{3}$$

B. Impedance/admittance LTI modelling

As discussed in [11], once the impedance measurements have been performed for a converter-based device, an LTI approximation of the apparent impedance of the system formed by the converter-based device and the grid's equivalent Thévenin impedance can be obtained applying the vector fitting algorithm [22]–[24] to assess possible instabilities. While this approach is useful for design purposes in a single converter, it remains impractical to assess instabilities in a larger grid with several converter-based devices. For power system's stability assessment, it is instead necessary to have a LTI representation of the converter-based device on its own. With such LTI representation in the dq domain, the converter dynamics could be incorporated in the state-space representation of the rest of the grid to perform standard eigenvalue and participation factor analysis. While this is possible, additional considerations must be taken care of when performing the vector fitting of the converter dynamics.

The vector fitting algorithm allows to obtain an LTI approximation $\hat{H}(s)$ for the set of frequency response measurements $\mathcal{F} = \left\{H(f_1), \ldots, H(f_{N_f})\right\}$. The approximation $\hat{H}(s)$ is a sum of rational functions as defined in (4), where a_i and b_i correspond to real residues and poles, while r_i and p_i are imaginary residues and poles respectively and D is a real constant. The outputs of the vector fitting algorithm are the residues and poles a_i, r_i, b_i and p_i together with D and the root mean square error ϵ_{rms} in relation to the input measurement set $\mathcal{F}$. The inputs to the vector fitting algorithm are [11]:

1) The set of frequency response measurements $\mathcal{F}$.
2) The desired order of the approximation defined as N.

The previous input arguments should be selected such that the RMS error ϵ_{rms} is minimized given a reasonable order of approximation N. In the next sections, a detailed overview is given on how these inputs should be selected.

$$\hat{H}(s) = D + \sum_{i=1}^{M}\left(\frac{a_i}{s - b_i}\right) + \sum_{i=M+1}^{N}\left(\frac{r_i}{s - p_i} + \frac{\bar{r}_i}{s - \bar{p}_i}\right) \tag{4}$$

1) Input frequency response measurements: While in most of the literature the impedance behaviour of converter-based devices is selected to perform stability analysis, this might not be the best choice to perform the LTI modelling of the converter dynamics. This can be understood if the sum of rational functions $\hat{H}(s)$ obtained from the vector fitting algorithm is translated into its rational polynomial form $P(s)/Q(s)$, where $P(s)$ and $Q(s)$ are polynomial functions of s with coefficients $\{a_1, \ldots, a_N\}$ and $\{b_1, \ldots, b_N\}$ respectively. With this representation, the impedance behaviour is represented by a rational matrix as shown in (5), where the argument (s) of each function has been omitted for clarity. This in turn means that, if the impedance behaviour $\mathbf{Z}_{dq}$ of the converter dynamics can be approximated by a sum of rational function of order N, then its admittance behaviour $\mathbf{Y}_{dq}$ defined by (6) will require an approximation of $4N$ if no zeros/poles cancellations occur. This implication goes both ways, i.e. if the admittance can be approximated by a sum of rational functions of order N, then its impedance behaviour will require an approximation of order $4N$.

This analysis indicates that when approximating the black-box converter dynamics using the vector fitting approach, both the impedance and admittance behaviours should be considered. Since no information is known from the internal dynamics of the device, it is not possible to know *a priori* which of the two representations will require the lowest order to approximate. In fact, it is possible that, while one representation can be accurately approximated using a sum of rational functions, its counterpart might be intrinsically not well-behaved to be fitted. A simple example of such case is when considering an RL circuit in the dq domain, where its impedance defined by (7) is not well-behaved for the purpose of rational fitting since it is improper, i.e. the order N_p of its numerator $P(s)$ is higher than the order N_q of its denominator $Q(s)$. Traditional vector fitting is able to approximate improper functions up to a second order difference, i.e. $N_p = N_q + 2$, by finding constants D and E. In the case of (7) however, the fitting process will add fictitious poles no matter the desired approximation order N defined by the user, introducing false dynamics and generating an inaccurate fitting of the original impedances. The admittance behaviour defined by (8) is proper and thus well-behaved for the purpose of vector fitting. The converter dynamics should thus be represented by the LTI model that has the lowest error for the desired fitting order N. As will be described in Section III, both the impedance and admittance LTI representations of the converter dynamics can be used for system-wise stability assessment studies.

$$\mathbf{Z}_{dq} = \begin{bmatrix} \frac{P_{dd}}{Q_{dd}} & \frac{P_{dq}}{Q_{dq}} \\ \frac{P_{qd}}{Q_{qd}} & \frac{P_{qq}}{Q_{qq}} \end{bmatrix} \tag{5}$$

$$\Leftrightarrow \mathbf{Y}_{dq} = \frac{1}{K}\begin{bmatrix} P_{qq}Q_{dd}Q_{dq}Q_{qd} & -P_{dq}Q_{dd}Q_{qq}Q_{qd} \\ -P_{qd}Q_{dd}Q_{qq}Q_{dq} & P_{dd}Q_{qq}Q_{dq}Q_{qd} \end{bmatrix} \tag{6}$$

$$\text{Where } K = \frac{1}{P_{dd}P_{qq}Q_{dq}Q_{qd} - P_{dq}P_{qd}Q_{dd}Q_{qq}}$$

$$\mathbf{Z}_{RL} = \begin{bmatrix} R + sL & -\omega_0 L \\ \omega_0 L & R + sL \end{bmatrix} \tag{7}$$

$$\mathbf{Y}_{RL} = \frac{1}{\left(R + sL\right)^2 + \left(\omega_0 L\right)^2}\begin{bmatrix} R + sL & \omega_0 L \\ -\omega_0 L & R + sL \end{bmatrix} \tag{8}$$

Another important aspect to consider in the vector fitting process is the dependence that the frequency response input data in the dq domain has on the angle δ_i for each i^{th} converter used for their synchronization via PLL. While frequency decoupled models, such as an RL branch, will have dq representations which are dq invariant, frequency-coupled models such as converter-based devices must be computed on a common dq reference frame [11], [25]. This can be achieved by using a linear transformation $\mathbf{T}_{dq,i}$ on the converter's measured impedance $\mathbf{Z}_i$ frequency response data by considering a common reference angle δ_{ref} and its synchronizing angle δ_i which can be computed from load flow calculations or by performing the FFT on the voltage signal of phase a when performing the frequency sweep measurements to obtain the impedance/admittance behaviour of the converter [11], to obtain the impedance frequency response $\tilde{\mathbf{Z}}_i(s)$ in the common reference frame as defined in (9). An analogous process can be performed for the measured admittance response.

$$\begin{aligned}\tilde{\mathbf{Z}}_i(s) &= \mathbf{T}_{dq,i}\mathbf{Z}_i(s)\mathbf{T}_{dq,i}^{-1} \\ \mathbf{T}_{dq,i} &= \begin{bmatrix} cos(\delta_i - \delta_{ref}) & -sin(\delta_i - \delta_{ref}) \\ sin(\delta_i - \delta_{ref}) & cos(\delta_i - \delta_{ref}) \end{bmatrix}\end{aligned} \tag{9}$$

When each dq impedance component is vector fitted independently, each element of the matrix $\mathbf{Z}_{dq}$ will have its own set of poles and residues as shown in (5). By combining (5) and (9), it is possible to see that, for a rational representation in a given dq reference frame $\mathbf{Z_{dq}}$, when translating it to another reference frame $\tilde{\mathbf{Z}}_{\mathbf{dq}}$ the order N and dynamics of the new rational representation will change. More specifically, each element of the new matrix $\tilde{\mathbf{Z}}_{\mathbf{dq}}$ will be a linear combination of the rational representations of $\mathbf{Z_{dq}}$, with scaling factors depending on the phase angle difference between the two dq reference frames being considered. This reference frame angle dependence can be avoided by identifying the common poles of all 4 components using the vector fitting process in the sum of them as defined in (10). Indeed, by performing the vector fitting algorithm to Z_{DQ} to obtain its rational approximation $\hat{Z}_{DQ}$, a common set of poles $\{\lambda_1, \ldots, \lambda_N\}$ defined by the denominator Q_Z can be derived for the impedance behaviour $\mathbf{Z_{dq}}$. Once the poles are identified, the residues of each element can be computed by performing the vector fitting on each element's frequency response data considering the poles previously computed, which will provide the polynomial functions P_{DD}, P_{DQ}, P_{QD} and P_{QQ}. This in turn provides a rational representation as shown in (12), which can be rotated from one dq reference to another using (9) without changing the order N of the approximation and the common set of poles $\{\lambda_1, \ldots, \lambda_N\}$, only the residue of its elements. It is thus concluded that the impedance and admittance elements in the dq domain should not be fitted independently if the dq reference frame rotation dependence of its LTI representation is to be minimized. This analysis is valid for both the impedance and admittance representations of the converter dynamics.

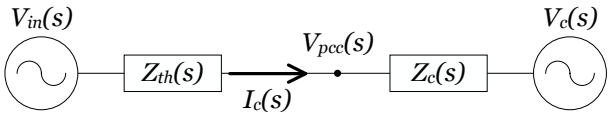


Fig. 2. Impedance representation of the measurement system.

$$Z_{DQ}(s) = Z_{dd} + Z_{dq} + Z_{qd} + Z_{qq} \tag{10}$$

$$\hat{Z}_{DQ}(s) \approx \frac{1}{Q_Z}\left(P_{DD} + P_{DQ} + P_{QD} + P_{QQ}\right) \tag{11}$$

$$\mathbf{Z}_{dq} = \frac{1}{Q_Z}\begin{bmatrix} P_{DD} & P_{DQ} \\ P_{QD} & P_{QQ} \end{bmatrix} \tag{12}$$

2) Approximation order selection: When selecting the approximation order N, in general the higher it is, the lower the RMS error ϵ_{rms} will be. However, it is not possible to select an arbitrarily large value of N. In this case, the order of the converter's impedance (or admittance) fitted approximation $Z_c(s)$, is constrained by the requirement of having a stable representation of the original measuring system as shown in Fig. 2. While the vector fitting algorithm can be set to always provide stable LTI representations, i.e. $b_i < 0\ \forall i \in \{1, \ldots, M\}$ and $\Re(p_i) < 0\ \forall i \in \{1 + M, \ldots, N\}$, the fitted approximation of the converter dynamics must fulfill that the complete measuring system is also stable. The dynamics of the complete measuring system are defined by (13). This in turn means that the approximation order N must be increased to reduce the RMS error ϵ_{rms} while providing stable representations of the original measuring system, i.e. the poles of $H(s)$ should be on the left half of the complex plane. The best LTI representation will thus be the one with the lowest RMS error while preserving the stable behaviour of the original measuring system. The fitting methodology is summarized in Fig. 3 for the admittance case, where it is shown how the fitting order should be increased until finding the first unstable model that signals the stopping criterion so that only the previous stable representation with the lowest RMS error is considered. The same process applies for the impedance behaviour of the converter. Large approximation orders will lead to over-fitting, which when evaluated in the original test system may lead to a false unstable representation.

$$\begin{aligned} V_{pcc}(s) &= H(s)\left[Y_{th}(s)V_{in}(s) + Y_c(s)V_c(s)\right] \\ H(s) &= \left(Y_c(s) + Y_{th}(s)\right)^{-1} \end{aligned} \tag{13}$$

With the previous considerations, it is thus possible to obtain an LTI representation of the converter dynamics in the dq domain, based either in the converter's impedance or admittance frequency response. In the next section, a detailed description is provided on how to integrate this LTI representation for power system stability assessment studies.

III. Impedance-based stability assessment

In this section, a detailed description on how to use the LTI impedance/admittance representation of black-box converter

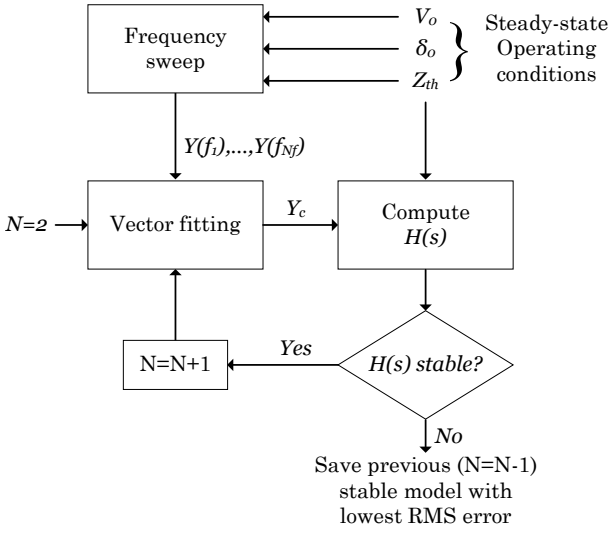


Fig. 3. Fitting methodology for the admittance frequency measurements.

models in stability assessment studies is provided. To this end, it is necessary to provide a framework that allows computing the state-space LTI representation of a power systems in the dq domain, including the converter's LTI models, to perform standard eigenvalue analysis of the system dynamics.

Once the converter's LTI model has been computed according to the methodology presented in Section II, its state-space representation can be computed. It is important to note that for the residue/pole representation obtained from the vector fitting algorithm, there are infinitely many possible state-space representations, most of which might not have any meaningful physical interpretation. However, it is possible to compute a circuit realization of both the impedance and admittance LTI models using RLC branches as shown in Fig. 4. The circuit parameters can be computed from the pole/residue values based on the relationships in [26], which are summarized for the admittance case in equations (14), (15) and (16). Analogous equations for the impedance realization can be found in [26].

$$R_0 = D \tag{14}$$

$$i \in \{1, ..., M\}: \quad \begin{cases} L_i = \frac{1}{a_i} \\ R_i = \frac{-b_i}{a_i} \end{cases} \tag{15}$$

$$i \in \{M+1, ..., N\}: \quad \begin{cases} L_i = \frac{1}{r_i + \bar{r}_i} \\ R_i = -\frac{r_i p_i + \bar{r}_i \bar{p}_i}{(r+\bar{r}_i)^2} \\ C_i = \frac{(r_i+\bar{r}_i)^4}{p_i \bar{p}_i (r_i+\bar{r}_i) - (r_i r_i + \bar{r}_i \bar{p}_i)(r\bar{p}_i + \bar{r}_i p_i)} \\ R_i' = \frac{-1}{C_i} \frac{r_i+\bar{r}_i}{r_i \bar{p}_i + \bar{r}_i p_i} \end{cases} \tag{16}$$

Using Kirchhoff's laws on the circuit realizations in Fig. 4, a state-space representation for the converter's impedance/admittance LTI model can be computed. For the case of the admittance representation, the aggregated state-space form of the 4 LTI models $Y_{dd}(s)$, $Y_{dq}(s)$, $Y_{qd}(s)$ and $Y_{qq}(s)$ is presented in (17). A similar procedure can be performed for the impedance representation, where the inputs

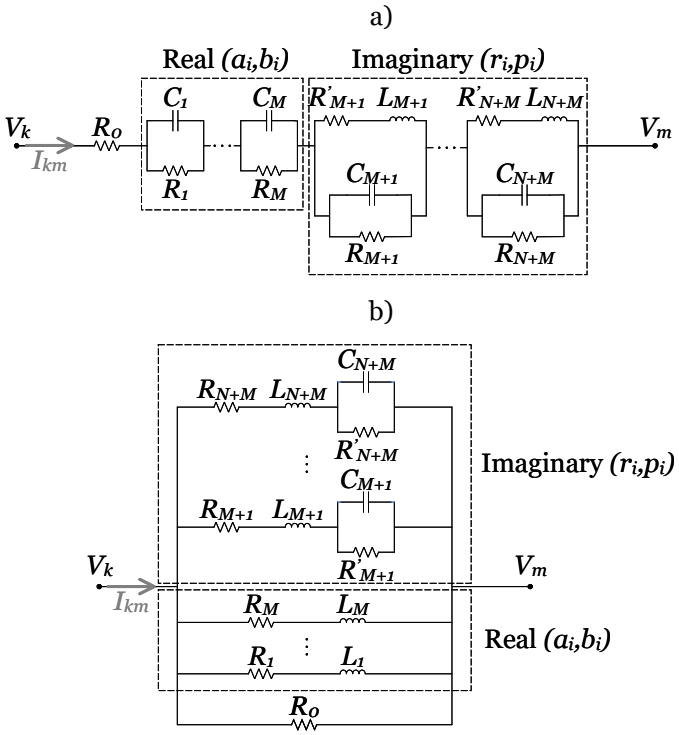


Fig. 4. Circuit realization of converter's LTI model for: a) impedance case, b) admittance case

are the currents $[I_{km,d}\ I_{km,q}]^t$ and the outputs are the voltage drops $[\Delta V_d\ \Delta V_q]^t$.

$$\begin{aligned} s \begin{bmatrix} X_{dd} \\ X_{dq} \\ X_{qd} \\ X_{qq} \end{bmatrix} &= \begin{bmatrix} A_{dd} & & & \\ & A_{dq} & & \\ & & A_{qd} & \\ & & & A_{qq} \end{bmatrix} \begin{bmatrix} X_{dd} \\ X_{dq} \\ X_{qd} \\ X_{qq} \end{bmatrix} \\ &+ \begin{bmatrix} B_{dd} & \\ & B_{dq} \\ B_{qd} & \\ & B_{qq} \end{bmatrix} \begin{bmatrix} \Delta V_d \\ \Delta V_q \end{bmatrix} \\ \begin{bmatrix} I_{km,d} \\ I_{km,q} \end{bmatrix} &= \begin{bmatrix} C_{dd} & C_{dq} & & \\ & & C_{qd} & C_{qq} \end{bmatrix} \begin{bmatrix} X_{dd} \\ X_{dq} \\ X_{qd} \\ X_{qq} \end{bmatrix} \\ &+ \begin{bmatrix} D_{dd} & D_{dq} \\ D_{qd} & D_{qq} \end{bmatrix} \begin{bmatrix} \Delta V_d \\ \Delta V_q \end{bmatrix} \end{aligned} \tag{17}$$

Once all state-space models have been computed for all converter-based devices of interest, they can be further aggregated to compute the state-space form of the entire grid in the dq frame. This can be done by first establishing one state-space representation for all branch element connections between busbars, and another state-space model for all shunt element connections from each busbar to ground.

For shunt connections to ground, the input signals are the currents $I_{b,dq}$ flowing from the grid to ground, while the output signals corresponds to the busbar's voltages V_{dq}. This state-space model accounts, for example, for the loads in the system and transmission lines' capacitances/conductances. The state-space representation is presented in (18).

For series elements connecting busbars/voltage sources, such as the converter's impedances/admittances, the series branches of transmission lines and transformers, they can be represented in a separate state-space model. In this case, the input signals are the voltage drops ΔV_{dq} between the connected busbars, including the input voltages to the gird $V_{in,dq}$ set by voltage sources such as synchronous machines or VSC converters. The output signals correspond to the flowing currents $I_{km,dq}$ on each series branch of the system. The state-space representation is presented in (19).

$$\begin{cases} sX_V = A_V X_V + B_V I_{b,dq} \\ V_{dq} = C_V X_V + D_V I_{b,dq} \end{cases} \tag{18}$$

$$\begin{cases} sX_I = A_I X_I + B_I \Delta V_{dq} \\ I_{km,dq} = C_I X_I + D_I \Delta V_{dq} \end{cases} \tag{19}$$

By combining (18) and (19), together with the nodal and branch balancing matrices ξ_I and ξ_V as defined in (20) (21), it is possible to establish a grid state-space representation. More specifically, the dynamic state-space matrix A_{sys} defining the dynamic behaviour of the grid can be computed according to (22). Using eigenvalue analysis and participation factor computation on A_{sys}, it is possible to identify unstable operating conditions and poorly damped oscillatory modes in the system, together with the respective contributions of each converter-based device. This assessment allows to take corrective measures, by changing the operating conditions and/or the control parameters of the converter-based devices. In addition, the impedance/admittance model of converter devices allows to easily reduce and aggregate them into equivalent impedance-voltage source representations at the fundamental frequency when they are electrically distant of the area or devices of interest in very large power systems, using standard impedance equivalence methods. In a large, realistic power system, when checking for converter interactions or poorly damped oscillations, in general, only a subset of power converters in a specific area of interest needs to be modelled in detail while the rest of the grid can be simplified. This procedure however becomes more complex as black-box models are considered in the grid, since their aggregation and reduction are not obvious and many times not possible to perform. Once the impedance modelling has been done however, this allows to reduce the original system and thus make stability assessment scalable to larger and more complex grids.

$$I_{b,dq} = \xi_I I_{km,dq} \tag{20}$$

$$\Delta V_{dq} = \xi_V V_{dq} + \xi_{in} V_{in,dq} \tag{21}$$

$$A_{sys} = \begin{bmatrix} A_V & \\ & A_I \end{bmatrix} + \begin{bmatrix} B_V \xi_I & \\ & B_I \xi_V \end{bmatrix} \begin{bmatrix} I & -D_I \xi_V \\ -D_V \xi_I & I \end{bmatrix}^{-1} \begin{bmatrix} & C_I \\ C_V & \end{bmatrix} \tag{22}$$

IV. Results

To test the methodologies proposed in Sections II and III, the well-known 39 Bus New England system, shown in Fig. 5, is implemented in PSCAD. All synchronous generators except for G1 include theirs governor, steam turbine and AVR models. The system is modified by replacing G9 in Bus 29 by a 200 MVA detailed type 4 VSC aggregated windfarm model, available in [27]. Transmission lines are modelled using Π - sections, and loads are modelled using an exponential model, with active power loads represented by a constant current characteristic and reactive power loads with a constant impedance characteristic.

To validate the proposed impedance stability assessment methodology, it is first tested to compare the stability boundaries between the average and detailed models of a MMC STATCOM module. Then, the proposed impedance stability assessment methodology is tested in the 39 Bus New England system for two scenarios:

- Scenario 1: to assess the dynamic behaviour of the windfarm for different values of the grid strength at Bus 26
- Scenario 2: to assess the risk of control interactions when connecting a 200 MVA MMC STATCOM at Bus 28

When performing stability assessment studies in large grids, it might be impractical to model in detail the entirety of the network. Depending on the phenomena being studied, different partition and reduction techniques have been developed in the literature, such that the model complexity can be reduced without significantly affecting the accuracy of the study [28]–[30]. More recent works have proposed power system clustering and partitioning based on electrical distance and grid topology, useful for voltage related studies [28], [29]. While reduction techniques are out of the scope of this work, the 39 Bus system is partitioned as proposed in [29] to perform the proposed LTI stability assessment based on the state-space representation of the grid. More specifically, devices in the subsystem under study are modelled in detail using their LTI models, while the rest of the grid is aggregated into equivalent Thévenin models at the subsystem's boundary busbars.

To perform stability assessment for both scenarios, the following methodology steps are performed:

1) Obtain the impedance frequency response for windfarm/STATCOM models as per Section II-A using the frequency sweep method on detailed EMT PSCAD models.
2) Obtain the LTI representation of each converter-based device as per Section II-B.
3) Perform eigenvalue analysis as per Section III, using a reduced representation of the system considering subsystem 2 and an equivalent Thévenin grid of the rest of the grid as seen from busbar 26, as shown in Fig. 6.
4) Validate stability assessment results with time-domain simulations in PSCAD in both the reduced 3 bus and full 39 bus systems.

A. MMC STATCOM model comparison

In this section, the proposed impedance modelling methodology is used to compute the stability boundary of a full-bridge MMC STATCOM module of 200 MVA. A detailed model is used, based on the HVDC model available in [31], which has been modified accordingly to work as a STATCOM model.

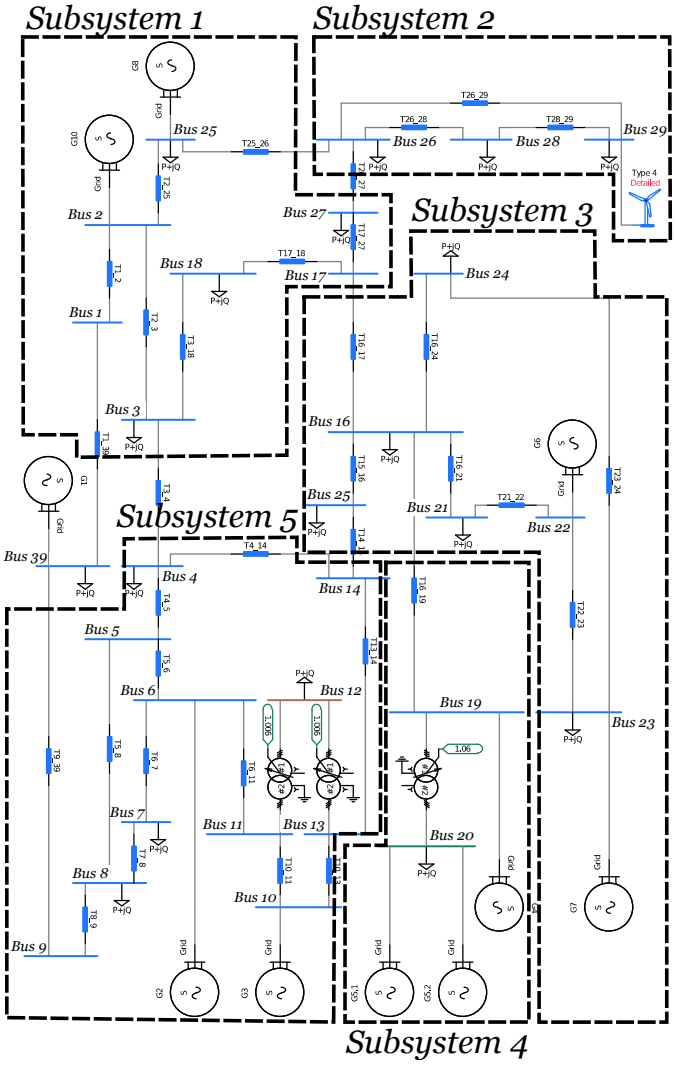


Fig. 5. Modified 39 Bus New England system in PSCAD, partitioned according to [29].

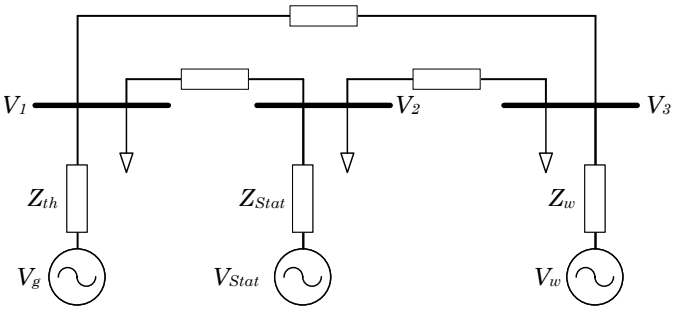


Fig. 6. Reduced equivalent of subsystem 2 for stability assessment.

TABLE I
MMC STATCOM PARAMETERS

Parameters	Value
Rated power	200 [MVAr]
Number of power modules	44 per arm
Power module capacitance	5 [mF] (17 kJ/MVA)
Arm inductance	20 [mH]
DC rated voltage	35.2 [kV]
AC rated voltage	33 [kV]
Carrier frequency	360 [Hz]

The STATCOM parameters are specified in Table I. The MMC detailed model considers:

- Standard dq PI vector control for the outer AC voltage and inner current control loops.
- PLL and PWM modulation for operating the power modules.
- Capacitor balancing is achieved by incorporating a sorting algorithm depending on the state of charge of each power module.
- A circulating current suppression control.

The proposed impedance modelling methodology is used to compare the stability boundaries between the average and detailed models of the MMC STATCOM module. The average model in this case considers:

- PLL control.
- Inner dq current control loop.
- Ideal constant DC voltage.

Both models are operating in AC voltage control mode, with a voltage reference of 1.0 p.u. and providing 100 MVAr. Initially, the impedance frequency response data is measured using the frequency sweep technique for both models. An LTI representation of each model is then computed in the dq domain as explained in Section II. It is worth noting that it is possible to obtain a good approximation of the admittance response for both the average and detailed models of the MMC STATCOM, but not when considering their impedance behaviour. This can be seen in Fig. 7 and Fig. 8, where the frequency response data for both MMC STATCOM models are shown, together with their respective vector fitting approximations. As it can be see from Fig. 7 and Fig. 8, while it is possible to obtain a good approximation of the admittance response with an approximation of order 6, the same cannot be said for the impedance response as opposed to the conventional approach presented in the literature. Indeed, whether the impedance or the admittance behaviour of the converter is best suited for the vector fitting procedure will depend on the internal control structure of the converter, on its control parameters and operating condition. The RMS fitting errors for each component for both models are summarized in Table II, where it is possible to see that the impedance fittings have a significantly larger error than the admittance ones. Only the magnitudes of the frequency response are shown due to space constraint, but similar results are obtained for the phase angle data. This goes in line with the theoretical description provided in Section II-B1.

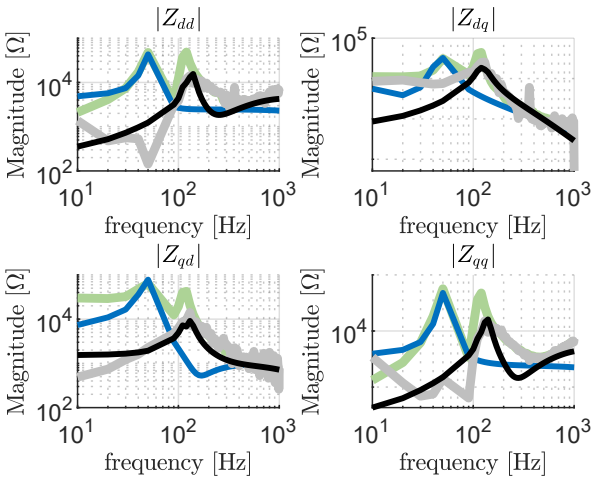


Fig. 7. Impedance frequency response for MMC STATCOM: in grey the measured data-points using the frequency sweep method for the detailed model and in green for the average model, together with their LTI vector fitting results in solid black and solid blue lines respectively.

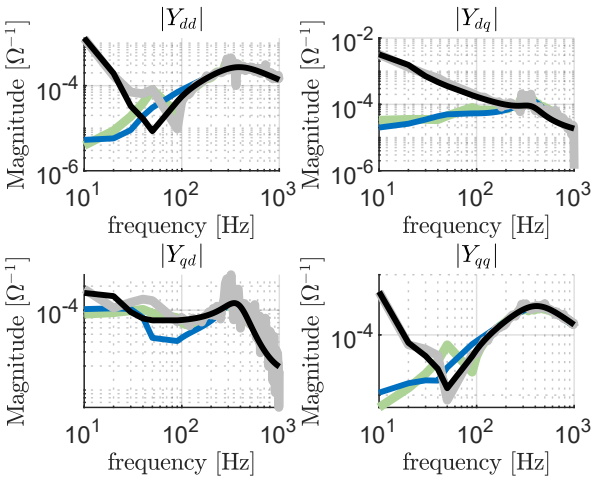


Fig. 8. Admittance frequency response for MMC STATCOM: in grey the measured data-points using the frequency sweep method for the detailed model and in green for the average model, together with their LTI vector fitting results in solid black and solid blue lines respectively.

TABLE II
RMSE FOR ADMITTANCE AND IMPEDANCE FITTINGS CONSIDERING DETAILED AND AVERAGED MMC STATCOM MODELS

	dd	*dq*	*qd*	*qq*
Y_{det}	5.287e-5	6.236e-5	4.713e-5	2.332e-5
Y_{avg}	3.481e-5	2.068e-5	2.216e-5	1.828e-5
Z_{det}	3.525e3	2.745e3	1.637e3	3.333e3
Z_{avg}	8.632e3	7.811e3	8.462e3	8.628e3

Using the LTI representations of both the detailed and average models, their stability boundaries can be computed for different values of the short-circuit ratio (SCR) and X/R ratio of the grid at the PCC. The stability boundary is useful for TNOs when assessing the risk of instability for converter-based devices due to an unexpected change in the short-circuit level or X/R ratio of the grid at the PCC, which typically happens after the clearance of a transmission line following a fault event. The stability boundary is computed in a similar way as done in the vector fitting technique shown in Fig. 3, by varying the values of the equivalent grid's inductance L_{th} and resistance R_{th} according to the desired SCR and X/R ratio defined as inputs. The SCR and X/R ratio would be defined based on prior knowledge of the system, i.e. its topology and plausible planned and unplanned outages/fault scenarios. For each value, the poles of the transfer function $H(s)$ as defined in equation (13) are computed. The L_{th}-R_{th} pair is then classified as a stable or unstable operating condition depending on the presence of poles with positive real part. The stability boundary regions for both models are shown in Fig. 9. As it is possible to see from Fig. 9, the average model greatly overestimates the stability boundary of the MMC STATCOM module, having the same control parameters as the detailed model but only considering the PLL and current control loops. It is also worth noting that for high SCR values, the average model will lead similar results to the detailed model and so in these conditions it would be enough for stability analysis.

To validate the stability boundaries shown in in Fig. 9, time domain simulations are performed in PSCAD and shown in Fig. 10, for both operating points 1 and 2. Initially the MMC STATCOM module is operating in steady-state condition with a short-circuit ratio (SCR) of 4.5 and an X/R ratio of 15. In the simulation for operating point 2, at 0.2 s the SCR is decreased to 0.335 as defined in Fig. 9. As it is possible to see, in this case the system is able to reach a new marginally stable steady-state condition with poorly damped oscillations that persist in the voltage and power signals. In the simulation for operating point 1, at 0.2 s the SCR is decreased from 4.5 to 0.327, which initially triggers poorly damped oscillations which eventually drive the system to becoming unstable after 1.3 s, thus representing a marginally unstable operating condition. It is also worth noting that the stability boundary computed considering the average model considers both operating condition as stable, which highlights the need to consider the full detailed model of the MMC STATCOM.

It is important to note that the LTI model obtained using the proposed methodology remains accurate only within the vicinity of the operating condition under which the impedance/admittance behaviour was measured during the frequency sweep. Indeed, if the stability boundary of the converter is to be computed accurately, the frequency sweep measurement should be performed in an operating condition close to the boundary. While in most cases the stability boundary is unknown, it can be computed by using the proposed methodology iteratively. First, an initial guess of the stability boundary can be computed by considering the LTI model obtained with measurements on a standard operating condition or any other stable operating condition. Then, a

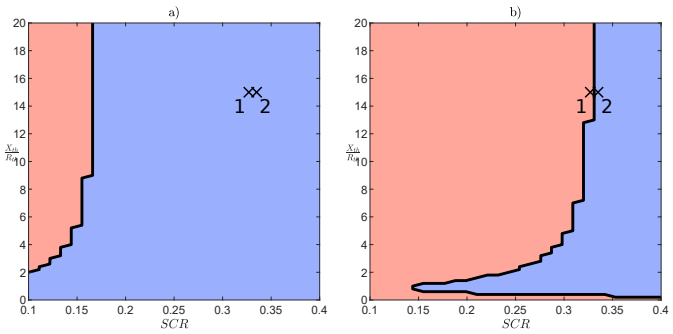


Fig. 9. Stability boundary for a) average and b) detailed MMC STATCOM models respectively. In red unstable operating region, in blue stable operating region. Point 1 represents a marginally unstable condition and point 2 a marginally stable one.

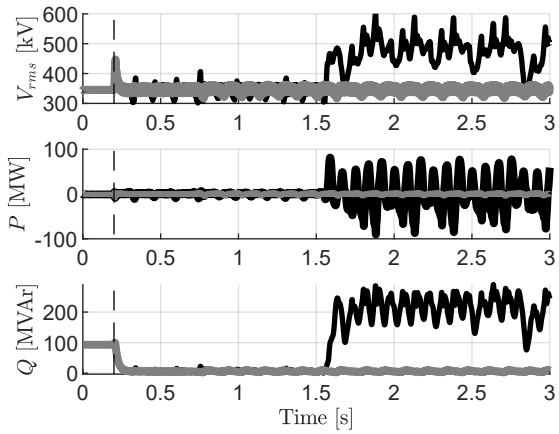


Fig. 10. Time-domain simulations in PSCAD for a sudden change in short-circuit level considering the MMC STATCOM mode: in grey for operating condition 2 and in black for operating condition 1.

more accurate prediction can be obtained by repeating the methodology but considering the measurements done on an operating condition close to the currently predicted boundary. By repeating this process iteratively and updating the stability boundary each step, an accurate estimation together with an accurate LTI model on its vicinity can be achieved. In the authors experience 2 or 3 iterations are sufficient to have accurate models and predictions.

B. Scenario 1 stability analysis

In scenario 1, a 200 MVA windfarm model is connected to Bus 29, providing 200 MW to the system. Its stability margin is computed for different values of the short-circuit level S_{SC} of the grid at busbar 26, the boundary busbar of subsystem 2 to the rest of the grid. The goal is to identify at which short-circuit level the VSC aggregated windfarm model loses stability. First, the frequency response of the windfarm model is measured in the dq domain as per the methodology presented in Section II-A. From these measurements, an LTI representation is obtained using the vector fitting technique using the methodology presented in Section II-B, the results are shown for the magnitude of its admittance response in Fig. 11.

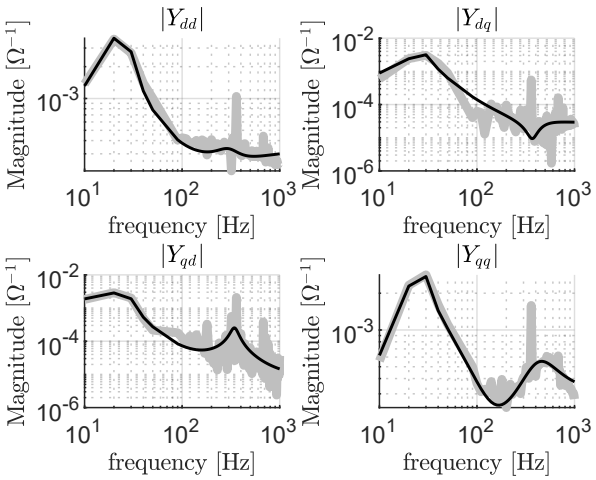


Fig. 11. Admittance frequency response for windfarm: in grey the measured data-points using the frequency sweep method, together with its LTI vector fitting results in solid black line.

Using the LTI representation of the windfarm, a state-space representation of subsystem 2 is obtained by reducing the rest of the grid by its short-circuit Thévenin equivalent at busbar 26. The original value starts at 3700 MVA, and it is reduced progressively by scaling the grid's Thévenin impedance Z_{th} at busbar 2631 while keeping the voltage at the busbar constant. For each value of the grid's short-circuit level S_{SC}, eigenvalue analysis is performed on the system dynamic matrix A_{sys} to identify possible unstable operations, i.e. poles with positive real part. The system's eigenvalue loci of interest are plotted in Fig. 12. As it is possible to see from Fig. 12, once the short-circuit level drops below 620 MVA, the windfarm can no longer remain stable.

The eigenvalue analysis is validated by performing time-domain simulations in PSCAD. The simulation are performed on the reduced 3 Bus system using the grid's Thévenin equivalent, since modifying the short-circuit level on the original 39 Bus system by changing the operating point and topology is cumbersome. The results for short-circuit levels of 620 and 530 MVA are shown in Fig. 13. Initially, the system is ramped-up to the steady-state operating condition and at time 0.5 [s] the windfarm model is deblocked, switching from zero output powers to its full detailed model at rated operating conditions. As it is possible to see from Fig. 13, the eigenvalue analysis considering the proposed LTI admittance modelling of the windfarm model accurately predicts the loss of stable operation once the short-circuit level drops to 530 MVA. For a grid strength of 620 MVA, the windfarm is able to transition into its steady-state operation with a poor dynamic response since there is a pair of poorly damped modes. Once the grid strength drops to 530 MVA, the windfarm is not able to transition into a stable steady-state operation.

C. Scenario 2 stability analysis

Once again, the proposed stability assessment methodology is applied to the reduced 3 Bus system, now incorporating the impedance LTI model of the MMC STATCOM. More

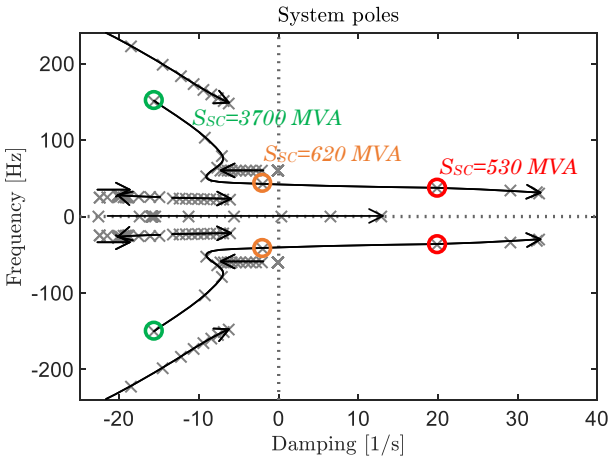


Fig. 12. 3 Bus system pole loci for different short-circuit levels of the grid at bus 26.

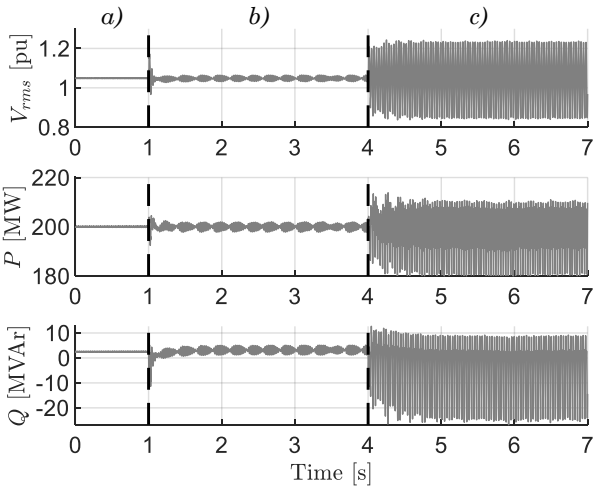


Fig. 13. Time-domain simulations in PSCAD for: a) $S_{sc} = 3700$ [MVA], b) $S_{sc} = 620$ [MVA] and c) $S_{sc} = 530$ [MVA]

specifically, the STATCOM module is operating in AC voltage control mode, injecting 100 MVAr to the grid at bus 28. The windfarm model is operating by injecting 200 MW to the grid at bus 29. A sensitivity analysis is performed on the proportional gain K_p of the AC outer voltage control loop of the STATCOM module. The gain K_p is varied from its base value of 0.5 to 2, 6, 10 and 20 in 6 different cases. For each gain value, a different LTI impedance model of the STATCOM is computed, i.e. a frequency sweep is performed, together with the vector fitting identification procedure and its associated state-space modelling is calculated. In each case, the 3 bus system's dynamic matrix A_{sys} is computed and the poles of the system are identified using eigenvalue analysis. The poles' loci of interest are shown in Fig. 14 where it is possible to see that once the proportional gain K_p increases to a value of 6, unstable operation should be expected.

To validate the results obtained using the proposed stability assessment methodology, time-domain simulations are performed on the entire 39 Bus system. The results for a proportional gain of 2 and 6 are shown in Fig. 15. The simulation is started from a steady-state condition with a proportional gain of $K_p = 0.5$, and at 0.5 [s] it is switched to $K_p = 6$ and $K_p = 2$ for the grey and black plots respectively. As it is possible to see from Fig. 15, when switching to a proportional gain of 2, the system is able to remain in steady-state operation and no significant change is seen in the outputs of the windfarm and STATCOM modules. Once the gain is increased to 6 however, stability is lost and both the STATCOM and windfarm are unable to control its output voltage and reactive power correctly.

It is worth noting that, since both the windfarm and STATCOM modules are stable independently, which is a condition necessary to perform the frequency sweep measurements, they are unstable when interconnected and the proportional gain is increased to 6. This is thus an unstable behaviour due to control interactions between the STATCOM module and windfarm model in close proximity. This is further verified when considering the participation factors of each model to the unstable mode, computed from the dynamic matrix A_{sys}, as shown in Fig. 16. As it is possible to see from Fig. 16, as the proportional gain increases and the dynamics performance worsens, both the STATCOM and windfarm models contribute to the unstable mode. While the contribution of the windfarm remains rather constant, the STATCOM's contribution increases with the AC gain as expected, since it is driving the unstable voltage behaviour. This analysis can be further disaggregated by each dq component contribution as shown in Fig. 17, for different values of the STATCOM AC voltage gain. As it is possible to see from Fig. 17, the main contribution to the unstable mode from the MMC STATCOM comes from its Y_{dq} component, which has the most significant increase in its participation factor as the AC proportional gain increases and the dynamic performance worsens. This is expected, since the vector control strategy in both the MMC STATCOM and windfarm modules use the q component of the voltage to control reactive power injection to the system. More specifically, the main contribution of the STATCOM module for a proportional gain of $K_p = 6$ comes from a state with an associated pole $p_1 = -55.78 \pm j109.9$ and a participation factor of 1.26% from its admittance LTI representation. This pole p_1 has thus associated frequencies in the dq domain of 17.5 Hz, smaller than $2f_0$ which in turn means that the corresponding states have a dynamic response in the subsynchronous frequency band as defined in [32]. As explained in detail in [32], these subsynchronous frequencies are associated with the converters' AC voltage control loop, which validates the results obtained from the eigenvalue and participation factor analysis performed using the proposed impedance-based stability assessment methodology.

V. Conclusions

In this paper, a comprehensive impedance-based stability assessment methodology for power system with converter-based devices is proposed. The methodology aims to fill the gap between impedance-based models and state-space representations for converter-based devices. This in turn provides a method to assess the risk of possible unstable operation for black-box converter models.

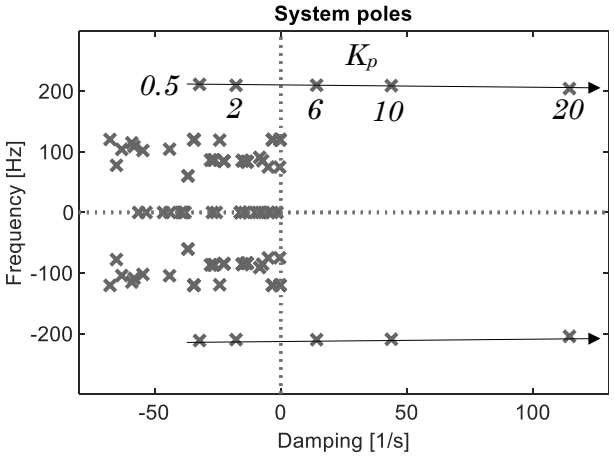


Fig. 14. 3 Bus system pole loci for different STATCOM AC voltage proportional gains K_p.

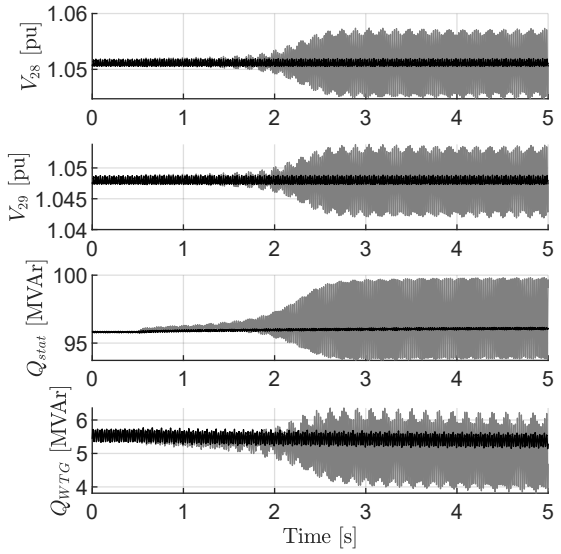


Fig. 15. Time-domain simulations in PSCAD: in grey for a STATCOM AC voltage proportional gain $K_p = 6$; in solid black line $K_p = 2$.

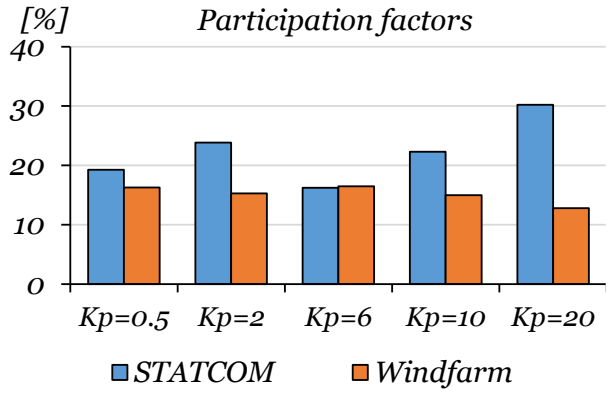


Fig. 16. Participation factors for different STATCOM AC voltage proportional gains K_p.

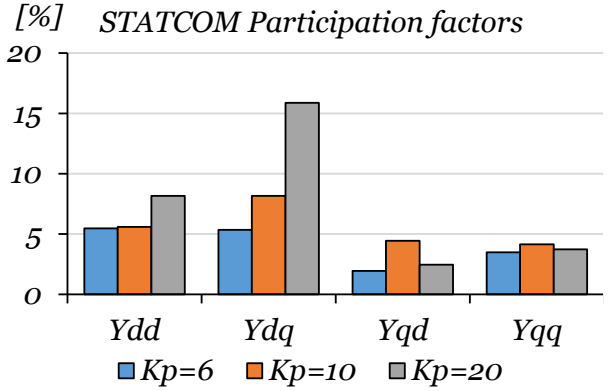


Fig. 17. Participation factors for STATCOM admittance dq components for an AC voltage gain of $K_p = 6$, $K_p = 10$ and $K_p = 20$.

The proposed methodology describes how to obtain an LTI representation of the converter's dynamics based on frequency response measurements. This is achieved by using the vector fitting algorithm on the impedance frequency response of the converter, measured using a frequency sweep technique. Using the LTI representation obtained from the vector fitting technique, a circuit realization using RLC branches is constructed, which can in turn be incorporated in the state-space model of a larger network. Using this state-space representation, dynamic operation can be assessed using traditional eigenvalue analysis and participation factor computation. The proposed methodology is able to handle both average and detailed models of both a aggregated VSC windfarm model and an MMC STATCOM module. The methodology is validated with EMT time-domain simulation in PSCAD on the 39 Bus New England System, considering detailed VSC windfarm and MMC STATCOM models. As future work, it would be necessary to validate the proposed impedance state-space modelling methodology with experimental results.

ACKNOWLEDGMENT

This work was funded as part of the National Grid Electricity Transmission UK NIA project "Risk Mitigation of Power Electronics Connections" (NIA_NGTO045)

REFERENCES

[1] J. Quintero, V. Vittal *et al.*, "The impact of increased penetration of converter control-based generators on power system modes of oscillation," *IEEE Trans. Power Syst.*, vol. 29, no. 5, pp. 2248–2256, 2014.

[2] Y. Li, L. Fan, and Z. Miao, "Wind in weak grids: Low-frequency oscillations, subsynchronous oscillations, and torsional interactions," *IEEE Trans. Power Syst.*, vol. 35, no. 1, pp. 109–118, 2020.

[3] N. Hatziargyriou, J. V. Milanovic *et al.*, "Definition and classification of power system stability revisited extended," *IEEE Trans. Power Syst.*, pp. 1–1, 2020.

[4] B. Wen, D. Boroyevich *et al.*, "Analysis of d-q small-signal impedance of grid-tied inverters," *IEEE Trans. Power Electron.*, vol. 31, no. 1, pp. 675–687, 2016.

[5] X. Wang, L. Harnefors, and F. Blaabjerg, "Unified impedance model of grid-connected voltage-source converters," *IEEE Trans. Power Electron.*, vol. 33, no. 2, pp. 1775–1787, 2018.

[6] C. Li, R. Burgos *et al.*, "Stability analysis of power systems with multiple statcoms in close proximity," *IEEE Trans. Power Electron.*, vol. 35, no. 3, pp. 2268–2283, 2020.

[7] Y. Gu, Y. Li *et al.*, "Impedance-based whole-system modeling for a composite grid via embedding of frame dynamics," *IEEE Trans. Power Syst.*, vol. 36, no. 1, pp. 336–345, 2021.
[8] X. Wang, F. Blaabjerg, and P. C. Loh, "Passivity-based stability analysis and damping injection for multiparalleled vscs with lcl filters," *IEEE Trans. Power Electron.*, vol. 32, no. 11, pp. 8922–8935, 2017.
[9] M. Cespedes and J. Sun, "Impedance modeling and analysis of grid-connected voltage-source converters," *IEEE Trans. Power Electron.*, vol. 29, no. 3, pp. 1254–1261, 2014.
[10] A. Rygg and M. Molinas, "Apparent impedance analysis: A small-signal method for stability analysis of power electronic-based systems," *IEEE Journal of Emerging and Selected Topics in Power Electronics*, vol. 5, no. 4, pp. 1474–1486, 2017.
[11] A. Rygg, M. Molinas *et al.*, "A modified sequence-domain impedance definition and its equivalence to the dq-domain impedance definition for the stability analysis of ac power electronic systems," *IEEE Journal of Emerging and Selected Topics in Power Electronics*, vol. 4, no. 4, pp. 1383–1396, 2016.
[12] Y. Li, Y. Gu *et al.*, "Impedance circuit model of grid-forming inverter: Visualizing control algorithms as circuit elements," *IEEE Trans. Power Electron.*, vol. 36, no. 3, pp. 3377–3395, 2021.
[13] J. Huang, K. A. Corzine, and M. Belkhayat, "Small-signal impedance measurement of power-electronics-based ac power systems using line-to-line current injection," *IEEE Trans. Power Electron.*, vol. 24, no. 2, pp. 445–455, 2009.
[14] V. Valdivia, A. Lázaro *et al.*, "Impedance identification procedure of three-phase balanced voltage source inverters based on transient response measurements," *IEEE Trans. Power Electron.*, vol. 26, no. 12, pp. 3810–3816, 2011.
[15] T. Roinila, T. Messo, and E. Santi, "Mimo-identification techniques for rapid impedance-based stability assessment of three-phase systems in dq domain," *IEEE Trans. Power Electron.*, vol. 33, no. 5, pp. 4015–4022, 2018.
[16] M. Raza, E. Prieto-Araujo, and O. Gomis-Bellmunt, "Small-signal stability analysis of offshore ac network having multiple vsc-hvdc systems," *IEEE Trans. Power Del.*, vol. 33, no. 2, pp. 830–839, 2018.
[17] Y. Gu, N. Bottrell, and T. C. Green, "Reduced-order models for representing converters in power system studies," *IEEE Trans. Power Electron.*, vol. 33, no. 4, pp. 3644–3654, 2018.
[18] J. Lyu, X. Zhang *et al.*, "Harmonic state-space based small-signal impedance modeling of a modular multilevel converter with consideration of internal harmonic dynamics," *IEEE Trans. Power Electron.*, vol. 34, no. 3, pp. 2134–2148, 2019.
[19] J. Kwon, X. Wang *et al.*, "Harmonic interaction analysis in a grid-connected converter using harmonic state-space (hss) modeling," *IEEE Trans. Power Electron.*, vol. 32, no. 9, pp. 6823–6835, 2017.
[20] M. Amin and M. Molinas, "A gray-box method for stability and controller parameter estimation in hvdc-connected wind farms based on nonparametric impedance," *IEEE Trans. Power Electron.*, vol. 66, no. 3, pp. 1872–1882, 2019.
[21] S. Lefteriu and A. C. Antoulas, "On the convergence of the vector-fitting algorithm," *IEEE Transactions on Microwave Theory and Techniques*, vol. 61, no. 4, pp. 1435–1443, 2013.
[22] B. Gustavsen and A. Semlyen, "Rational approximation of frequency domain responses by vector fitting," *IEEE Trans. Power Del.*, vol. 14, no. 3, pp. 1052–1061, July 1999.
[23] B. Gustavsen, "Improving the pole relocating properties of vector fitting," *IEEE Trans. Power Del.*, vol. 21, no. 3, pp. 1587–1592, July 2006.
[24] D. Deschrijver, M. Mrozowski *et al.*, "Macromodeling of multiport systems using a fast implementation of the vector fitting method," *IEEE Microwave and Wireless Components Letters*, vol. 18, no. 6, pp. 383–385, June 2008.
[25] Y. Gu, Y. Li *et al.*, "Impedance-based whole-system modeling for a composite grid via embedding of frame dynamics," *IEEE Trans. Power Syst.*, vol. 36, no. 1, pp. 336–345, 2021.
[26] G. Antonini, "Spice equivalent circuits of frequency-domain responses," *IEEE Transactions on Electromagnetic Compatibility*, vol. 45, no. 3, pp. 502–512, Aug 2003.
[27] [Online]. Available: https://www.pscad.com/knowledge-base/article/227
[28] E. Cotilla-Sanchez, P. D. H. Hines *et al.*, "Multi-attribute partitioning of power networks based on electrical distance," *IEEE Trans. Power Syst.*, vol. 28, no. 4, pp. 4979–4987, 2013.
[29] I. Tyuryukanov, M. Popov *et al.*, "Discovering clusters in power networks from orthogonal structure of spectral embedding," *IEEE Trans. Power Syst.*, vol. 33, no. 6, pp. 6441–6451, 2018.
[30] ——, "Slow coherency identification and power system dynamic model reduction by using orthogonal structure of electromechanical eigenvectors," *IEEE Trans. Power Syst.*, vol. 36, no. 2, pp. 1482–1492, 2021.
[31] [Online]. Available: https://www.pscad.com/knowledge-base/article/234
[32] X. Wang and F. Blaabjerg, "Harmonic stability in power electronic-based power systems: Concept, modeling, and analysis," *IEEE Transactions on Smart Grid*, vol. 10, no. 3, pp. 2858–2870, 2019.



Nicolás Cifuentes (M'19) was born in Santiago, Chile. He received the B.S. and M.S. degrees in electrical engineering from the University of Chile, Santiago, in 2017. He is currently pursuing the Ph.D. degree with the Control and Power Group, Department of Electrical and Electronic Engineering, Imperial College London. His main interests are power systems' dynamic modeling, control and stability, dynamic impact and control strategies in large-scale integration of converter-based technologies for power generation and FACT devices.



Mingyu Sun (Member, IEEE) received the B.Eng. degree in electrical engineering from Shandong University, Jinan, China, in 2013, and the M.Sc. and Ph.D. degrees in electrical power engineering from The University of Manchester, Manchester, U.K., in 2014 and 2020, respectively. He is currently a senior engineer with the National Grid ESO, U.K. From Sept 2019 to August 2021, he was an innovation engineer with National Grid Electricity Transmission, U.K., leading innovation projects on power electronics and its control interactions. His research interests include application of power electronics in power systems, and wide-area monitoring, protection, and control systems.



Robin Gupta received a master's degree in electrical engineering from IIT Kanpur, India in 2008. He is working with National Grid Electricity Transmission, UK, as Net Zero innovation Manager. In this role, he is leading a research team to develop the cost-effective and reliable future electricity transmission network. Before joining National Grid, he led several engineering and R&D projects on converter control system design, power system modelling and smart grid with GE and Siemens. He is a chartered engineer with IET and IAM certified in asset management.



Bikash C. Pal (M'00-SM'02-F'13) received B.E.E. (with honors) degree from Jadavpur University, Calcutta, India, M.E. degree from the Indian Institute of Science, Bangalore, India, and Ph.D. degree from Imperial College London, London, U.K., in 1990, 1992, and 1999, respectively, all in electrical engineering. Currently, he is a Professor in the Department of Electrical and Electronic Engineering, Imperial College London. His current research interests include renewable energy modelling and control, state estimation, and power system dynamics. He is Vice President Publications, IEEE Power & Energy Society. He was Editor-in-Chief of IEEE Transactions on Sustainable Energy (2012-2017) and Editor-in-Chief of IET Generation, Transmission and Distribution (2005-2012) and is a Fellow of IEEE for his contribution to power system stability and control